Title
Reversible silencing of endogenous receptors in intact brain tissue using 2-photon pharmacology

Journal
Proceedings of the National Academy of Sciences of the United States of America, 116(27)

ISSN
0027-8424

Authors
Pittolo, Silvia
Lee, Hyojung
Lladó, Anna
et al.

Publication Date
2019-07-02

DOI
10.1073/pnas.1900430116

Peer reviewed

Reversible silencing of endogenous receptors in intact brain tissue using 2-photon pharmacology

Silvia Pittolo[a,1], Hyojung Lee[a], Anna Lladó[b], Sébastien Tosi[b], Miquel Bosch[a,2], Lídia Bardia[b], Xavier Gómez-Santacana[a,c,3], Amadeu Llebaria[c], Eduardo Soriano[d,e,f], Julien Colombelli[b], Kira E. Poskanzer[g,h], Gertrudis Perea[i], and Pau Gorostiza[a,e,j,4]

[a]Institute for Bioengineering of Catalonia (IBEC), Barcelona Institute of Science and Technology, 08028 Barcelona, Spain; [b]Institute for Research in Biomedicine (IRB Barcelona), Barcelona Institute of Science and Technology, 08028 Barcelona, Spain; [c]Institute of Advanced Chemistry of Catalonia, Consejo Superior de Investigaciones Científicas (IQAC-CSIC), 08034 Barcelona, Spain; [d]Department of Cell Biology, Physiology, and Immunology, University of Barcelona (UB), 08028 Barcelona, Spain; [e]Catalan Institution for Research and Advanced Studies (ICREA), 08010 Barcelona, Spain; [f]Network Center of Biomedical Research in Neurodegenerative Diseases (CIBERNED), 28031 Madrid, Spain; [g]Department of Biochemistry & Biophysics, University of California, San Francisco (UCSF), CA 94158; [h]Kavli Institute for Fundamental Neuroscience, University of California, San Francisco, CA 94158; [i]Cajal Institute, Consejo Superior de Investigaciones Científicas (IC-CSIC), 28002 Madrid, Spain; and [j]Network Center of Biomedical Research in Bioengineering, Biomaterials, and Nanomedicine (CIBER-BBN), 50015 Zaragoza, Spain

Edited by Ehud Y. Isacoff, University of California, Berkeley, CA, and approved May 16, 2019 (received for review January 14, 2019)

The physiological activity of proteins is often studied with loss-of-function genetic approaches, but the corresponding phenotypes develop slowly and can be confounding. Photopharmacology allows direct, fast, and reversible control of endogenous protein activity, with spatiotemporal resolution set by the illumination method. Here, we combine a photoswitchable allosteric modulator (alloswitch) and 2-photon excitation using pulsed near-infrared lasers to reversibly silence metabotropic glutamate 5 ($mGlu_5$) receptor activity in intact brain tissue. Endogenous receptors can be photoactivated in neurons and astrocytes with pharmacological selectivity and with an axial resolution between 5 and 10 μm. Thus, 2-photon pharmacology using alloswitch allows investigating $mGlu_5$-dependent processes in wild-type animals, including synaptic formation and plasticity, and signaling pathways from intracellular organelles.

photopharmacology | photoactivation | pharmacological selectivity | functional silencing | 2-photon pharmacology

Understanding the physiological function of a gene requires pinpointing the exact time course, spatial distribution, and functioning of the encoded protein, from cells to living organisms. This challenge is tackled with techniques based largely on gene targeting and pharmacology. Genetic methods transiently or permanently remove the target protein (knockout or knockdown) (1, 2), thus allowing us to spot the effects of protein loss in a genetically modified organism, but the actual control over the target is intrinsically limited to a timescale of hours to days (i.e., the time course of protein expression), and to the cellular specificity of the available molecular markers. Pharmacological blocking of receptor protein function does not reproduce accurately the complex physiology of receptors because spatially-restricted or dynamic control over their targets cannot be exerted (3). However, recently reported light-regulated drugs (photopharmacology or optopharmacology) can mimic complex receptor kinetics (4) and dynamics of cell-to-cell communication in intact brain tissue using patterns of illumination (5). Light drives reversible photoisomerization of such drugs from their active to inactive form and back, and allows turning protein function on and off at illuminated locations and timescales that match the kinetics of the receptor, such that the spatiotemporal resolution for protein switching is only limited by the illumination method.

Photopharmacology can be used in wild-type organisms to acutely block the target protein widely, and then "restore" it at any combination of locations and times defined by the illumination pattern. Thus, it allows scrutinizing the role of a protein from the consequences of its presence, instead of its absence, making this technique emerge as an alternative to classic pharmacology (which is limited by the timing required for drug application, diffusion, and removal) (6), as well as to genetic targeting (by avoiding physiological compensations and off-target effects often observed with these approaches) (7). The reported spatiotemporal precision of photopharmacology in manipulating neural circuits is comparable to that of optogenetics (8, 9), without the possible drawbacks of distorting cell physiology by overexpression and immunogenicity of microbial proteins (10, 11).

One major limitation of all current photopharmacological approaches is their application in 3D tissues. Our and other groups have developed, over the past years, a set of freely diffusible photopharmacological compounds that orthosterically or allosterically target different neurotransmitter receptors, such as ionotropic (12–15) and metabotropic glutamate receptors (16, 17), μ-opioid receptors (18, 19), $GABA_A$ receptors (20), nicotinic ACh receptors (21), and adenosine receptors (22), and could be

Significance

Two-photon fluorescent probes to image intracellular calcium and other biochemical processes have revolutionized cell biology. In neurobiology, 2-photon calcium indicators produce signals that indirectly reflect action potential firing in neurons deep in the brain, and have become essential to record and correlate large-scale neural activity at high spatiotemporal resolution. Here we show that 2-photon excitable, diffusible photoswitches allow the activation and deactivation of neurotransmitter receptors with higher subtype-specificity and spatial resolution compared with previous molecular tools, and combined with calcium indicators enables to both control and readout activity using 2-photon excitation. Specifically, we used a potent and selective antagonist to switch on/off at the micrometer scale the activity of $mGlu_5$ receptors expressed endogenously in neurons and astrocytes of intact brain tissue.

Author contributions: S.P., G.P., and P.G. designed research; S.P., H.L., M.B., K.E.P., and G.P. performed research; A. Lladó, S.T., L.B., X.G.-S., A. Llebaria, E.S., and J.C. contributed new reagents/analytic tools; S.P. and H.L. analyzed data; and S.P. and P.G. wrote the paper.

The authors declare no conflict of interest.

This article is a PNAS Direct Submission.

[1]Present address: Department of Biochemistry & Biophysics, University of California, San Francisco, CA 94158.

[2]Present address: Institute of Biomedical Research Agustí Pi i Sunyer (IDIBAPS), 08036 Barcelona, Spain.

[3]Present address: Institute of Functional Genomics, Université de Montpellier, Unité 5302 CNRS and Unité U1191, INSERM, 34090 Montpellier, France.

[4]To whom correspondence may be addressed. Email: pau@icrea.cat.

This article contains supporting information online at www.pnas.org/lookup/suppl/doi:10.1073/pnas.1900430116/-/DCSupplemental.

Published online June 13, 2019.

used to tackle important research questions in the field, but in practice none of the related published works clearly demonstrates the potential of this technique for activating neurotransmitter receptors with axial specificity.

The majority of these studies show that these molecules can be selectively turned on and off using illumination by single-photon excitation (1PE), which causes photon absorption throughout the optical axis, and thus photopharmacological drugs are photoisomerized in a large number of neurons at a time. The photostimulated volume can be reduced using pulsed illumination with femtosecond near-infrared (NIR) lasers (23), which enable 2-photon excitation (2PE) of photosensitive molecules to be constrained to physiologically relevant dimensions, such as dendritic spines or cell somata in circuits (24). Despite advances in 2PE of opsins (25), the axial selectivity that can be achieved using photopharmacology and 2PE is still unknown (15, 26, 27).

To photocontrol the activity of a specific receptor subtype with 3D resolution in a physiological context (e.g., in the brain), it is necessary to employ a photoswitchable ligand having the highest pharmacological selectivity. Currently, the best available option is to use alloswitch and its analog compounds, which are freely diffusible allosteric modulators of metabotropic glutamate 5 ($mGlu_5$) receptors (16, 28). These receptors are important modulators of neurotransmission and synaptic plasticity (29) and are involved in several neurological conditions (30–35). Alloswitch and its analogs are subtype-selective, allosteric ligands with nanomolar activity that can turn on and off endogenous $mGlu_5$ receptors in vivo. They exist in a thermodynamically stable, inhibitory *trans*-isomer that prevents receptor activation, and contain a light-sensitive moiety based on azobenzene (phenylazopyridine) that can be photoisomerized to its noninhibitory *cis* configuration using 1PE at visible wavelengths.

Here, we demonstrate that alloswitch can be efficiently photoisomerized using 2PE, we determine the axial resolution of this method, and we establish its feasibility in cultured cells and acute brain slices. This way, the pharmacological blockade of $mGlu_5$ is released exclusively using light, which offers an opportunity to silence $mGlu_5$ receptors widely, and then photoactivate them at selected locations and times. The rapid and reversible silencing of neurotransmitter receptors in rodent brain slices by 2PE of an allosteric photoswitch offers opportunities to study neuromodulation in intact neuronal circuits and 3D tissues with unprecedented pharmacological selectivity, tissue depth, and spatial resolution, and will be invaluable to understand how these receptors function in the unmodified brain.

Results

$mGlu_5$ Receptors Are Photocontrolled by Pulsed Light in "All-2PE" Experiments. To monitor and manipulate the activity of $mGlu_5$ receptors with 2PE of the freely diffusible drug alloswitch (Fig. 1*A*), we used an inverted laser-scanning microscope equipped with a pulsed NIR laser (*SI Appendix*, *Materials and Methods 2*). For the initial characterization, we overexpressed the $mGlu_5$ receptor fused to the fluorescent reporter eYFP in HEK cells (Fig. 1*B*). The activity of $mGlu_5$ can be monitored with fluorescence imaging of intracellular Ca^{2+} using chemical dyes and genetically encoded sensors, at both 1PE and 2PE. The expected wavelength for alloswitch isomerization at 2PE is around 780 nm (twice the optimal wavelength for 1PE, 390 nm) (16). Because switching the power of our NIR laser was faster than switching its wavelength during 2PE imaging and activation, we decided to monitor Ca^{2+} at 780 nm and low excitation intensity using the fluorescent Ca^{2+} indicator Fura-2 (Fig. 1*B*), which has a good absorption under pulsed NIR light (36) and no spectral overlap with the eYFP reporter (see *SI Appendix*, *Materials and Methods 3.3.3* and Fig. S1, regarding single-wavelength imaging with Fura-2). To photocontrol $mGlu_5$ activity, we bath-applied alloswitch along with an $mGlu_5$ agonist (quisqualate) to generate a "ready-steady-go" state in the cells (Fig. 1*A*) whereby, in the absence of illumination, the allosteric antagonist *trans*-alloswitch would put a brake to the intracellular Ca^{2+} events initiated by the $mGlu_5$ agonist, whereas its photoisomerization to the *cis*- (noninhibiting) isomer would prompt the onset of Ca^{2+} activity.

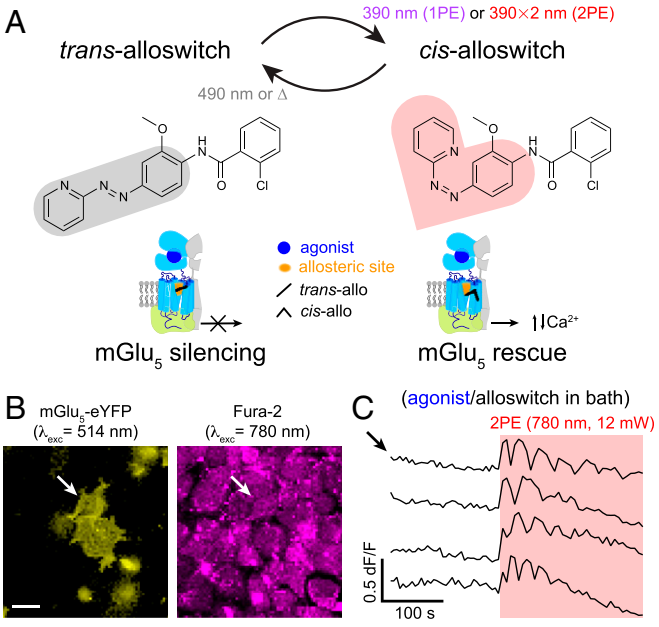

Fig. 1. Two-photon excitation of alloswitch at NIR wavelengths in cultured cells. (*A*, *Upper*) *Trans* → *cis* photoisomerization of alloswitch occurs by 1PE under violet light (390 nm). Using pulsed-lasers for 2PE, the expected wavelength for photoswitching is double that required for 1PE. Back-isomerization occurs by thermal relaxation (Δ; half-life of *cis*-isomer, $t_{1/2} = 80$ s) (16) or under 490-nm light. The photosensitive core of alloswitch, azobenzene, is highlighted in its *trans* (gray shade) and *cis* configurations (red shade). (*Lower*) *Trans*-alloswitch silences active, agonist-bound $mGlu_5$ receptors by binding at the allosteric pocket, whereas *trans* → *cis* photoisomerization of alloswitch rescues the silenced, agonist-bound receptors at the site of illumination by releasing intracellular, agonist-induced Ca^{2+} oscillations. (*B*) HEK cells expressing $mGlu_5$-eYFP (yellow, *Left*) and loaded with Fura-2 (magenta, *Right*) for 2-photon imaging of Ca^{2+} (760–820 nm; shown here is 780 nm). Arrows indicate cell shown by top trace in *C*. (Scale bar, 20 μm.) (*C*) Representative traces of Ca^{2+} oscillations induced by 2PE of alloswitch (1 μM) with quisqualate ($mGlu_5$ orthosteric agonist, 3 μM) in bath (arrow indicates trace for cell in *B*), and elicited by 2PE of alloswitch at 780 nm (red box; 12-mW scans) (see details on illumination patterns in *SI Appendix*, Fig. S1*C*). Ca^{2+} traces are shown as changes of Fura-2 fluorescence relative to baseline (dF/F; excited at 780 nm, 3 mW) (see direction of fluorescence changes of Fura-2 excited at 780 nm in *SI Appendix*, Fig. S1*A*). See corresponding trace of $mGlu_5$-eYFP$^-$ cell in *SI Appendix*, Fig. S1*F* and similar experiments for other alloswitch analogs in *SI Appendix*, Fig. S3.

After $mGlu_5$ inhibition was confirmed by silencing of responses to agonist (*SI Appendix*, Fig. S1*B*), we used a minimal laser power (3 mW, 780 nm) to visualize Ca^{2+} by 2PE-imaging of Fura-2, and an increased power (12 mW) to produce 2PE-isomerization of alloswitch to the noninhibiting *cis*-isomer, leading to cell activation (see strategy for achieving interleaved 2PE-imaging and 2PE-stimulation, named "all-2P experiments," and increased fluorescence of sample during photostimulation in *SI Appendix*, *Materials and Methods 3.3* and Fig. S1 *C–E*). Laser power was kept to minimal values for 2PE-imaging to minimize unwanted 2PE of alloswitch molecules due to imaging of Fura-2. We observed that 2PE raster scans at 780 nm, 12 mW, and 10-μs dwell time (*SI Appendix*, *Materials and Methods 2 and 3.3*) were sufficient to elicit $mGlu_5$-dependent intracellular Ca^{2+} oscillations, indicating efficient alloswitch photoisomerization and release of the "brake" exerted by alloswitch on the receptors (Fig. 1*C*). Note that all cells displaying Ca^{2+} oscillations under 2PE were eYFP$^+$ (*SI Appendix*, Fig. S1*F*), which indicates that responses were mediated by $mGlu_5$ and rules out artifacts due to photostimulation alone. To determine the optimal wavelength

for 2PE of alloswitch, we repeated "all-2PE" experiments at different spectral positions in the NIR range between 760 and 820 nm. Fura-2 allows 2PE fluorescence imaging of $mGlu_5$-dependent Ca^{2+} oscillations at all wavelengths in that range (*SI Appendix*, Fig. S1*A*), and can be combined with 2PE-isomerization of alloswitch at the same wavelengths (Fig. 2 and *SI Appendix*, Figs. S1*C* and S2). We found that 2PE at 780 nm produced the optimal photoisomerization of alloswitch. Although the maximum oscillatory frequency was lower at 780 nm than at 760 nm (Fig. 2, *Left*), oscillations at 780 nm lasted longer (Fig. 2, *Center Left*), were induced faster (Fig. 2, *Center Right*), and achieved more oscillatory events (Fig. 2, *Right*) despite a slightly lower laser power than that measured at 800 nm (*SI Appendix*, Fig. S2*E*). Several alloswitch analogs have been recently reported that display a variety of pharmacological and photophysical properties (28), and we selected a few to test their ability to photocontrol $mGlu_5$ receptors at 2PE. We repeated the same experiments using analogs bearing substitutions at the distal phenyl ring, and found that all of them were responsive at similar wavelengths (*SI Appendix*, Fig. S3).

Efficacy of 2PE and 1PE to Rescue Silenced $mGlu_5$ Receptors Using Alloswitch in HEK Cells. Two-photon excitation of molecules using pulsed lasers requires the coincident absorption of 2 photons and therefore occurs with lower probability than 1PE and mainly at the focal volume (23). In the case of photoswitches, this translates into generally lower isomerization efficacy at 2PE than at 1PE, even if photoisomerization quantum yields are unchanged (27). We set out to compare the efficacy of 2PE versus 1PE of alloswitch (Fig. 3*A*) by measuring responses repetitively and reproducibly in the same cell to avoid variability due to heterogeneity of receptor density and localization. For this purpose, we used the genetically encoded Ca^{2+} sensor GCaMP6s (37), whose excitation wavelength does not cross-excite alloswitch and allows longer experiments than Fura-2 without risk of photostimulation due to imaging. GCaMP6s was coexpressed in HEK cells with $mGlu_5$ receptors lacking the eYFP tag, to avoid fluorescence cross-talk (Fig. 3*B* and Movie S1). We activated $mGlu_5$ receptors by adding to the bath the agonist quisqualate (3 μM) and recorded the time course of Ca^{2+} responses (Fig. 3 *C*, *Left*). In cells displaying oscillatory behavior, the frequency of Ca^{2+} oscillation is proportional to the number of available $mGlu_5$ receptors (38). We then silenced $mGlu_5$ responses by addition of 1 μM alloswitch in the bath (Fig. 3 *C*, *Center*), and sequentially photostimulated cells in the field of view at 1PE and 2PE (Fig. 3 *C*, *Right*). We compared the efficacy of alloswitch to photoinduce $mGlu_5$-dependent Ca^{2+} oscillations at 1PE or 2PE relative to the endogenous activity of the receptor (expressed as oscillatory frequency of cells in response to agonist alone) (Fig. 3 *D*, *Left*), and found that 2PE produced oscillatory response frequencies that were 76 ± 11% of those induced by the agonist, and 53% of those induced by 1PE. Note that the oscillatory activity in response to 1PE of alloswitch was higher than in response to the applied agonist alone, as previously reported (16). Individual cells displaying oscillatory responses to both 1PE and 2PE allowed us to compare the fraction of $mGlu_5$ receptors photoactivated by 1PE and 2PE, being the number of expressed receptors and signal transduction machinery unchanged for a given cell within the time course of our experiments. We found that the frequency of oscillations with 2PE of alloswitch was 48 ± 4% of that obtained with 1PE in the same cell (Fig. 3 *D*, *Right*), which suggests that about half the receptors are recruited in the small 2PE volume compared with 1PE of the entire cell.

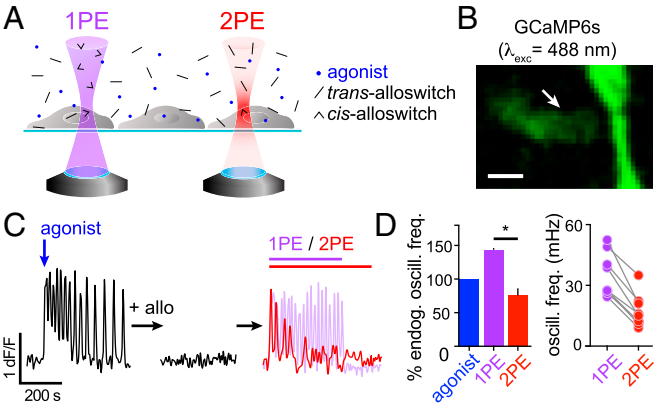

Fig. 3. Efficacy of $mGlu_5$ rescue by 1PE or 2PE of alloswitch in cultured cells. (*A*) Scheme of alloswitch photoactivation (*trans*: black sticks; *cis*: arrowheads) by 1PE and 2PE. Light-cones represent probability of efficient excitation of molecules by 1 (1PE, violet) or 2 coincident photons (2PE, red). Cells expressing $mGlu_5$ are supplemented with agonist (blue dots) and alloswitch, and light from an inverted confocal microscope is focused at the cell plane. Single-photon excitation excites molecules in solution along the entire light cone, whereas light from a pulsed laser excites molecules within its point spread function volume (for most 2P systems, 1 μm^3; for representation, 2PE spot is exaggerated compared with cell size). (*B*) Fluorescence of the Ca^{2+} sensor GCaMP6s (excited at 488 nm) in HEK cells. Arrow indicates cell in *C* (see also Movie S1). (Scale bar, 10 μm.) (*C*) Representative Ca^{2+} trace (GCaMP6s dF/F) from cell indicated by arrow in *B* in different conditions: in response to an $mGlu_5$ agonist (quisqualate, 3 μM; blue arrow; *Left*); after treatment with alloswitch (1 μM; *Center*); during photoactivation (*Right*) at 1PE (violet line and trace) or 2PE (red line and trace). See GCaMP6s imaging conditions (*SI Appendix, Materials and Methods 3.4*) and alloswitch photostimulation (*SI Appendix, Materials and Methods 5.2*). (*D*) Quantification of oscillatory Ca^{2+} events from experiments as in *C*. (*Left*) Percentage of Ca^{2+} oscillations frequency elicited by receptor activation with 1PE (violet bar, 144 ± 2%) or 2PE (red bar, 76 ± 11%) of alloswitch, relative to the endogenous oscillatory frequency generated by agonist alone acting on $mGlu_5$ receptors (blue). Dunn's multiple comparison test after the Friedman test for matched data; *$P < 0.05$. Data are mean ± SEM, $n = 4$ cells. (*Right*) Frequency of Ca^{2+} oscillations generated by 2PE of alloswitch was on average 48 ± 4% of that induced by 1PE in the same cell. Data are mean ± SEM; $n = 9$ cells from 2 independent experiments. Paired *t* test; $P < 0.0001$.

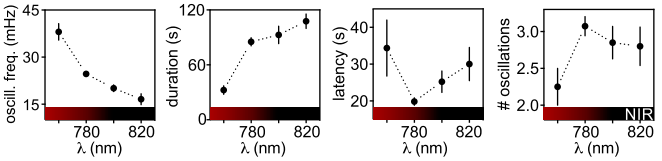

Fig. 2. Efficacy of responses with 2PE of alloswitch as a function of the pulsed laser wavelength. Experiments were conducted as in Fig. 1C, in HEK cells expressing $mGlu_5$-eYFP, loaded with Fura-2 for 2P-Ca^{2+} imaging, and supplemented with agonist (quisqualate, 3 μM) and alloswitch (1 μM) before experiments. Wavelength-dependence of frequency of Ca^{2+} oscillations (*Left*), duration of the oscillatory behavior (*Center Left*), time to first peak after 2PE onset (latency, *Center Right*), and number of oscillations observed during 2PE (*Right*). Oscillation frequency was higher after 2PE at 760 nm compared with other wavelengths (38.1 ± 2.6 mHz, $P < 0.05$) and at 780 nm compared with 820 nm (24.7 ± 0.7 mHz, $P < 0.001$). Duration was lower for 760 nm compared with other wavelengths (32.4 ± 4.7 s, $P < 0.05$). Data represent the mean ± SEM, $n = 4$–95 cells; Dunn's multiple comparison test after the Kruskal–Wallis test; see full statistic comparisons in *SI Appendix*, Fig. S2.

Silenced Receptors Are Rescued by 2PE of Alloswitch with Axial-Plane Selectivity in a Cell Monolayer. An advantage of 2PE over 1PE is that the former reduces out-of-focus excitation in the axial direction by orders of magnitude, restricting to micrometric volumes the excitation of molecules (23). This is well established in the case of fluorescent molecules, but it remains unexplored for photoswitchable compounds (15, 26, 27). Here, we asked whether alloswitch could be photoisomerized to its nonantagonizing *cis*-isomer with axial precision, despite diffusion of the inhibiting *trans*-isomer from outside the 2PE volume. To answer this question, we coexpressed $mGlu_5$ and GCaMP6s in HEK cells and repeated 1PE and 2PE at various axial distances above the cell

focal plane (Fig. 4 *A* and *B* and Movie S2). Cell responses to the receptor agonist were recorded, then alloswitch was applied to the bath to inhibit the induced Ca^{2+} oscillations (Fig. 4 *C*, *Left*). Single-photon excitation of alloswitch photoactivated cells regardless of the axial position of photostimulation, with the maximal distance tested 30 μm above cells (Fig. 4*C*). Of the total number of photoresponsive cells (displaying changes in intracellular Ca^{2+}) (faint colors in Fig. 4 *D*, *Upper*; see also classification methods and example traces in *SI Appendix*, *Materials and Methods* and Fig. S4 *C* and *D*), 66 ± 3% displayed oscillatory responses at both 0 and 30 μm (dark bars in Fig. 4 *D*, *Upper*, and *SI Appendix*, Fig. S4*E*). About 75% of cells that responded to 1PE were also photoactivated by 2PE at the cell plane (0 μm), and 24 ± 4% displayed oscillatory responses (Fig. 4 *D*, *Lower*; see also example traces in *SI Appendix*, Fig. S4 *C* and *D*). In contrast, photoisomerizing alloswitch with 2PE only 10 μm above the cell plane produced responses in only 17 ± 6% of cells, and none when the photostimulation plane was 30 μm above the cell focal plane (Fig. 4 *D*, *Lower*, and *SI Appendix*, Fig. S4*E*). We further quantified the frequency, oscillation number, onset time (latency), and duration of the Ca^{2+} responses, and found that 2PE at the cell plane elicited slightly lower frequencies, fewer oscillations, and longer latency than 1PE (42 ± 6 s, 27 cells), whereas response duration was similar for 2PE and 1PE (Fig. 4*E* and legend for values; see statistics in *SI Appendix*, Fig. S4*F*). Together, these results demonstrate that $mGlu_5$ photoactivation in a volume restricted by 2PE of alloswitch is possible despite diffusion of inhibiting *trans*-isomers into the 2PE volume. The axial resolution in our experimental conditions allows selective activation of $mGlu_5$ signaling within 10 μm of the target receptors. The fact that the basal cell surface in contact with the glass coverslip (0 μm) can be photoactivated more efficiently than the apical side exposed to the bath (10 μm) suggests that more receptors are photorescued at the basal side, probably because its flat shape matches better the 2PE plane than the curved contour of the apical side.

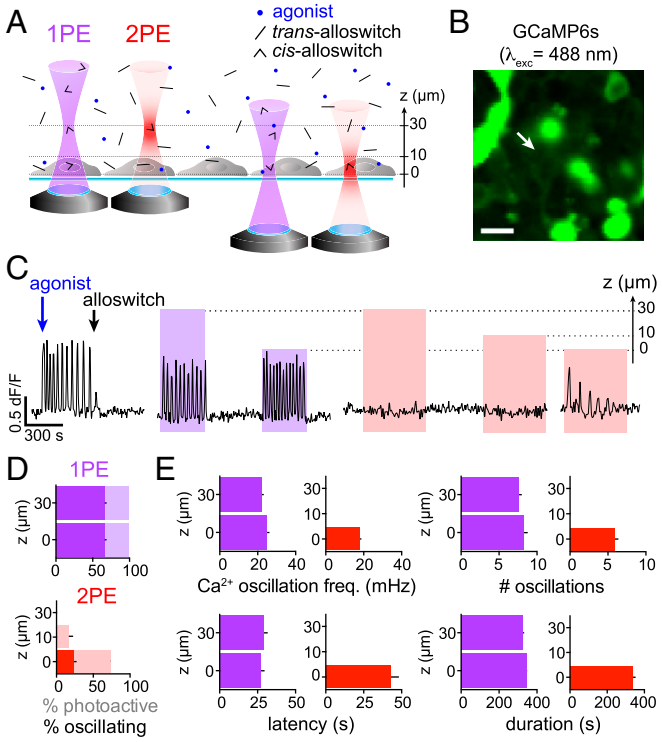

Fig. 4. Two-photon excitation of alloswitch in free-diffusion medium enables axially resolved photoactivation of $mGlu_5$. (*A*) Experimental design. Light is focused at different axial distances (Z = 30, 10, or 0 μm) upwards from the cell focal plane in an inverted microscope. Single-photon excitation of alloswitch stimulates $mGlu_5$ on cells at any axial distance, whereas 2PE of alloswitch is effective only when light is focused at the cell plane (Z = 0). (*B*) HEK cells expressing GCaMP6s for Ca^{2+} imaging. Arrow indicates cell recorded in *C* (Movie S2). (Scale bar, 20 μm.) (*C*) Representative trace (cell indicated by arrow in *B*) showing that photoactivation of Ca^{2+} responses occurs regardless of the focal plane with 1PE of alloswitch, and is focal-plane (Z = 0) -selective with 2PE. Ca^{2+} oscillations were elicited by $mGlu_5$ agonist (quisqualate, 3 μM; blue arrow) and blocked by alloswitch (1 μM; black arrow). Light for alloswitch excitation is focused above the Ca^{2+}-imaging plane at indicated axial distances (Z, μm). See imaging and stimulation conditions in *SI Appendix*. (*D*) Percentages of responsive cells with 1PE (*Upper*) or 2PE (*Lower*) at indicated Z positions, shown as percent of photoactive (positive Ca^{2+} changes; faint colors) and percent showing oscillatory behavior (solid colors). All photoactive cells responded to 1PE regardless of Z, and 66 ± 3% of them displayed an oscillatory phenotype. With 2PE at the focal plane (0 μm): photoactive cells, 73.0 ± 0.3%; oscillating cells: 24 ± 4% (36% of the cells found to oscillate at 1PE). With 2PE 10 μm above: photoactive cells, 17 ± 6%. Two-photon excitation at axial distances of 10 or 30 μm induced no oscillations. $n = 67$ cells from 2 independent experiments. See full dataset in *SI Appendix*, Fig. S4*E*. (*E*) Quantification of the oscillatory behavior of cells in *D* as Ca^{2+} oscillation frequency (*Upper Left*), number of oscillations (*Upper Right*), latency to the first oscillation after illumination onset (*Lower Left*), and overall duration (*Lower Right*). When photoactivating at Z = 0, the oscillation frequency was lower at 2PE than 1PE (18 ± 1 and 25 ± 1 mHz, respectively, $P < 0.01$), as well as the number of oscillations achieved (5.9 ± 0.5 and 8.3 ± 0.5, $P < 0.05$), whereas the latency was longer in trend (42 ± 6 and 27 ± 3 s, $P = 0.25$), and the duration unaffected. Cell responses were similar for 1PE at all axial distances. Data are mean ± SEM; Kruskal–Wallis test with Dunn's correction. Single-photon excitation, $n = 45$ from 2 independent experiments; 2PE, $n = 27$ from 3 independent experiments. See full dataset and statistics in *SI Appendix*, Fig. S4*F*.

Alloswitch Can be Used for Functional Silencing and Light-Induced Rescue of $mGlu_5$ Receptors in Acute Brain Slices. To test whether alloswitch can photocontrol endogenous $mGlu_5$ receptors expressed by both neurons and astrocytes in intact neural tissue, we set up photoswitching experiments in acute rodent brain slices while monitoring activity in both cell types using the Ca^{2+}-sensitive dye OGB-1 (Fig. 5 *A* and *B*). We used rat pups (postnatal days 6–15) due to the high expression of $mGlu_5$ receptors in neonatal (*SI Appendix*, Fig. S6*A*) compared with adult brain tissue (39), and we targeted the hippocampal CA1 region because of the documented $mGlu_5$ receptor expression in this brain area (40). We used a glass micropipette placed on top of the field-of-view for local delivery of the $mGlu_1$/$mGlu_5$ agonist DHPG by pressure-ejection (Fig. 5*B*). The circulating bath contained LY367385 to antagonize $mGlu_1$ responses, and tetrodotoxin (TTX) to prevent propagation of responses to neighboring neurons. Photostimulation of alloswitch and fluorescence imaging of OGB-1 were performed using the inverted confocal microscope setup described above (see illumination paradigm in *SI Appendix*, Fig. S5*A*). Because loading of OGB-1 is not cell-type–selective, recorded Ca^{2+} traces represent responses from a mixed population of neurons and astrocytes. After establishing Ca^{2+} responses of untreated cells to DHPG ejection (Fig. 5C; labeled "agonist," compared with OGB-1 fluorescence at rest, labeled "basal"), alloswitch was added to the bath (10 μM). The cellular responses mediated by $mGlu_5$ were silenced in the presence of *trans*-alloswitch (Fig. 5*C*, labeled "agonist/alloswitch"). Upon raster-scanning the field-of-view to photoisomerize alloswitch to the *cis*-isomer by 1PE, $mGlu_5$ responses to agonist ejection were readily rescued (Fig. 5*C*, labeled "ago + 1PE/alloswitch"). The time course of OGB-1 fluorescence from an example experiment (Fig. 5*D*, *SI Appendix*, Fig. S5*A*, and Movie S3), and counting of silent and responding cells (Fig. 5*E*) show that alloswitch and 1PE enable reversible silencing and light-induced rescue of $mGlu_5$ activity in brain slices. DHPG-responding cells drop from 19 to 2% in the presence of 10-μM alloswitch. Interestingly, during 1PE of alloswitch, Ca^{2+} responses were recovered in 31% of the cells in the field-of-view, a higher fraction ($P < 0.05$; paired *t* test) than observed before alloswitch application (Fig. 5*E*).

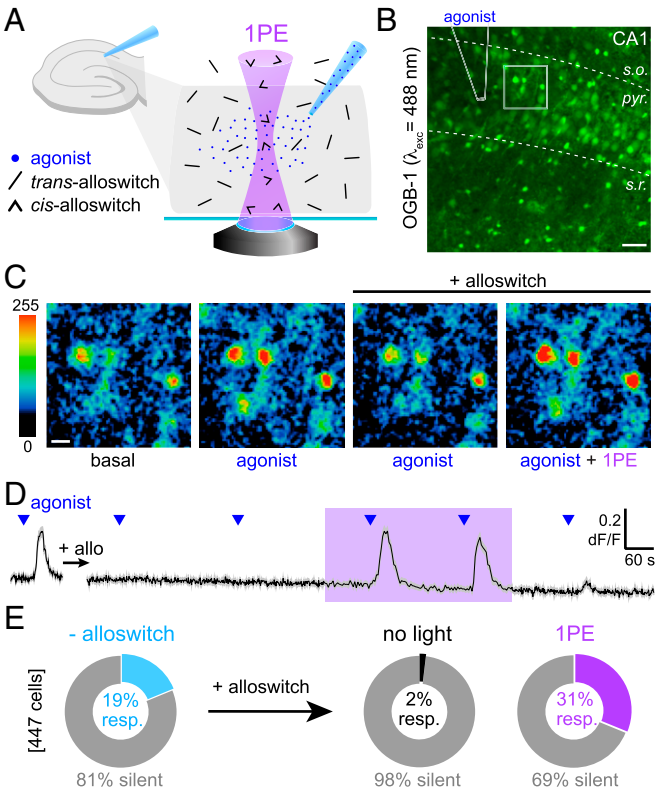

Fig. 5. Functional silencing and light-induced rescue of $mGlu_5$ receptors in acute brain slices. (*A*) Experimental design for the photoactivation of $mGlu_5$ in brain slices. A pipette filled with $mGlu_5$ agonist (DHPG, blue dots) is placed on the CA1 region of the hippocampus in a rat brain slice for cell stimulation. *Trans*-alloswitch in bath (blocks $mGlu_5$ responses to agonist) is photoconverted to *cis*-alloswitch ($mGlu_5$-block is released) along the light cone (violet, 1PE). (*B*) Fluorescence of cells bulk-loaded with OGB-1 for Ca^{2+} imaging in the CA1 of the rat hippocampus. Lines indicate strata (dashed: s.o., stratum oriens; s.r., stratum radiatum; pyr., stratum pyramidale) and pipette position (solid) for agonist ejection; square indicates region magnified in *C*. (Scale bar, 50 μm.) (*C*) Magnification of *B* in pseudocolors, illustrating the time course of Ca^{2+} responses at time 0 (*Left*), 40 s after agonist ejection in the absence (*Center Left*) or presence (*Center Right*) of alloswitch in the bath. Response during 1PE of alloswitch is shown 37 s after ejection (*Right*). (Scale bar, 10 μm.) (*D*) Average trace of Ca^{2+} responses to agonist ejected at times indicated by blue triangles (1 mM DHPG; 800 hPa, 1 s) acquired before (*Left*) and after (*Right*) addition of alloswitch in bath (+ allo, 10 μM), and during light stimulation in the 1PE regime (violet box, 405-nm laser diode, 58-μW power, 2.5-μs dwell time, and 0.3-Hz illumination rate). Data are mean fluorescence changes of OGB-1 (black) ± SEM (gray) from 39 cells initially responding to agonist. OGB-1 was excited at 488 nm, 2.4 μW, 0.3–1 Hz. See imaging/photostimulation protocol and control trace without alloswitch in *SI Appendix*, Fig. S5*A*. (*E*) Percentage of cells responding to agonist ejection in experiments as in *D*. Cells not responding to agonist puffing are shown as silent (gray). Cells responding to agonist before alloswitch treatment were 18.8 ± 0.8% (light blue, *Left*). The fraction of responding cells was reduced by addition of alloswitch (black, *Center*; 1.9 ± 1.0%, $P < 0.01$), and increased by 1PE (58–98 μW) of alloswitch (violet, *Right*; 31.2 ± 0.2%, $P < 0.05$; paired *t* test). Percentages calculated out of OGB-labeled cells in a 0.14-mm^2 area surrounding the pipette. Data are mean ± SEM; $n = 447$ cells from 2 animals.

Efficacy of 2PE of Alloswitch Is 30% of 1PE to Rescue Silenced $mGlu_5$ Receptors in Brain Slices. We next aimed to constrain $mGlu_5$ activation to the focal plane using 2PE in acute brain slices. We performed Ca^{2+} imaging experiments with LY367385, TTX, and alloswitch in the bath (Fig. 6*A*). The same cells were sequentially stimulated with DHPG before, during 2PE and 1PE of alloswitch, and after illumination (Fig. 6*B*, *SI Appendix*, Fig. S5, and Movie S4) (see also control experiments without alloswitch). Two-photon excitation successfully induced Ca^{2+} responses in 25% of cells in the imaged region compared with 76% of responses with 1PE; in addition, $mGlu_5$ events triggered by 2PE displayed 15% lower peak amplitude (Fig. 6 *C*, *Lower*) and were shorter than 1PE, suggesting a confined photoisomerization of alloswitch and limited number of recruited receptors under 2PE. In these experiments, the photoresponse latency measured after the agonist puff is 29 ± 2 s (83 cells). In control experiments, photostimulation periods in naïve slices (no alloswitch, no agonist ejection) (*SI Appendix*, Fig. S5*C*) had no effect on cytosolic Ca^{2+}. The efficacy of 2PE compared with 1PE of alloswitch in brain slices is in line with that observed in cultured cells (Fig. 3), suggesting that diffusion of alloswitch isomers in brain tissue is not a limiting factor in photocontrolling $mGlu_5$ receptor responses.

Axial Resolution to Activate Neurons and Astrocytes in Brain Slices by 2PE of Alloswitch Is Below 10 μm. Although the relevant parameter to evaluate the advantages of 2PE is the axial resolution achieved with a given compound, this value has not been determined for any of the previously reported azobenzene photoswitches, neither tethered (26, 27) nor freely diffusible (15). To calculate the axial resolution of 2PE of alloswitch in brain slices, we recorded the responses of cells in one plane (OGB-1 fluorescence, z_{img}) and compared the effect of photostimulation of alloswitch at 5

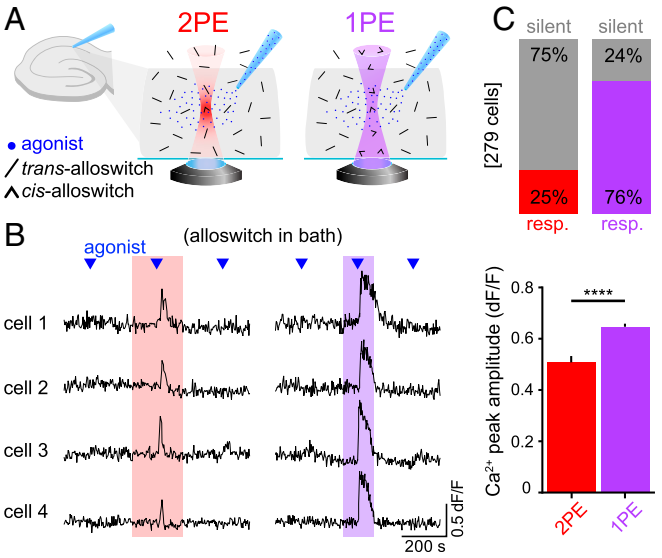

Fig. 6. Efficiency of $mGlu_5$ activation using 1PE and 2PE of alloswitch in a 3D tissue. (*A*) Schematics of the experimental design. *Trans*-alloswitch in bath ($mGlu_5$-block) is photoconverted to *cis*-alloswitch ($mGlu_5$-block is released) along the volume of brain slice illuminated by the light cone of 1PE (violet) or in the focal spot of 2PE (red). Pipette for delivery of $mGlu_5$ agonist (DHPG) is placed on top of imaged cells in the CA1 region of the hippocampus. (*B*) Example traces of 4 recorded cells with alloswitch in bath, comparing the Ca^{2+} responses to agonist puffing (blue triangles) before, during, and after 2PE (*Left*, red box) or 1PE (*Right*, violet box) of alloswitch. Single- and double-photon excitation were achieved with 2 (1PE) or 3 (2PE) consecutive raster scans at a frequency of 0.4 Hz and 0.26 Hz, respectively, with pixel dwell time of 2.5 μs, and laser power of 58 μW (1PE) and 25 mW (2PE). Ca^{2+} traces are shown as changes in OGB-1 fluorescence (dF/F; excited at 488 nm, 1.7–5.2 μW). See for imaging/photostimulation schematics and for control trace without alloswitch in *SI Appendix*, Fig. S5*B*. (*C*) Quantification of cell responses to agonist puffing from experiments as in *B*. (*Upper*) Percentage of responding (colored) and silent (gray) cells during 2PE (red) or 1PE (violet) of alloswitch. Cells are shown as percentages of the total number of OGB-1–labeled cells detected in the imaged area (0.1 mm^2). (*Lower*) The average peak amplitude of Ca^{2+} responses to 2PE in cells shown as responding in top graph ($n = 69$ cells, 3 animals) was about 15% lower (****$P < 0.0001$, unpaired *t* test) than the amplitude of 1PE responses ($n = 212$ cells, 3 animals). Data are mean ± SEM.

axial positions (z_{stim}) within 15 μm above and below the imaging plane (Fig. 7*A*). Additionally, the astrocytic marker sulforhodamine 101 (SR101) (Fig. 7 *B*, *Middle*) was included in the ejection pipette to identify responding cells as astrocytes or neurons (only labeled with OGB-1) (Fig. 7 *B*, *Top*). We first quantified photoresponses of all neurons and astrocytes. Single-photon excitation produced Ca^{2+} responses in the imaging plane regardless of the position of photostimulation plane (Fig. 7 *C*, *Right*), in agreement with the results observed in cell culture (Fig. 4). In contrast, 2PE responses were observed mostly when photostimulation was performed on the imaging plane (Fig. 7 *C*, *Left*, 0 μm), indicating that $mGlu_5$ receptors silenced with the *trans*-alloswitch (*SI Appendix*, Fig. S7) were selectively rescued by photoisomerizing alloswitch to the *cis* form in a confined region in the axial direction.

The Ca^{2+} responses to 1PE and 2PE were quantified as a function of the axial distance in 2 ways. First, the response amplitude expressed as relative change in fluorescence (%dF/F) was around 30% and did not change significantly with the distance for 1PE, whereas it showed a maximum of 20% at 0 μm for 2PE (Fig. 7*D*). Fitting 2PE data to a Gaussian function yielded a full-width half-maximum (FWHM, axial resolution) (*SI Appendix*, *Materials and Methods 6.4*) of 5.4 ± 0 μm. Second, the percentage of cells displaying photoresponses was ∼60% at any axial distance for 1PE, whereas 2PE responses were maximal at 0 μm (40% of cells) (Fig. 7*E*) and the FWHM of this Gaussian distribution was 10.3 ± 2.3 μm. Colabeling with SR101 indicated that about half of the cells (52%) responding to 1PE of alloswitch were astrocytes (*SI Appendix*, Fig. S6 *B–D*), supporting the use of alloswitch as a versatile tool to photocontrol different cell types in intact brain tissue. Cells responding to 2PE included a higher fraction of astrocytes (63%) but no differences between astrocytes and neurons were observed in the amplitude or time course of 1PE or 2PE responses in our experimental conditions (see example traces in *SI Appendix*, Fig. S6*C*).

Two-Photon Excitation of Alloswitch Allows Functional Mapping of $mGlu_5$ Receptors in CA1 Pyramidal Neurons. Previous studies localize the expression of $mGlu_5$ receptors to the dendritic arborization, but not the somata, of CA1 pyramidal neurons (40), whose proximal dendritic trees are divided into basal and apical branches, respectively located in the stratum oriens and radiatum of the hippocampus. Despite both regions receiving inputs from CA3, apical and basal dendrites of CA1 pyramidal neurons display unique synaptic properties (41), and some studies indicate that $mGlu_5$ receptors differentially modulate synaptic plasticity at these sites (42). All previous studies used pharmacological blockade to demonstrate the involvement of $mGlu_5$ receptors, but used field stimulation with extracellular electrodes to induce synaptic plasticity. Thus, the spatial extent of receptor activation is uncertain, and the recruitment of receptors other than $mGlu_5$ cannot be ruled out. Recent work found that local activation of $mGlu_5$ receptors by puffing DHPG through a glass micropipette

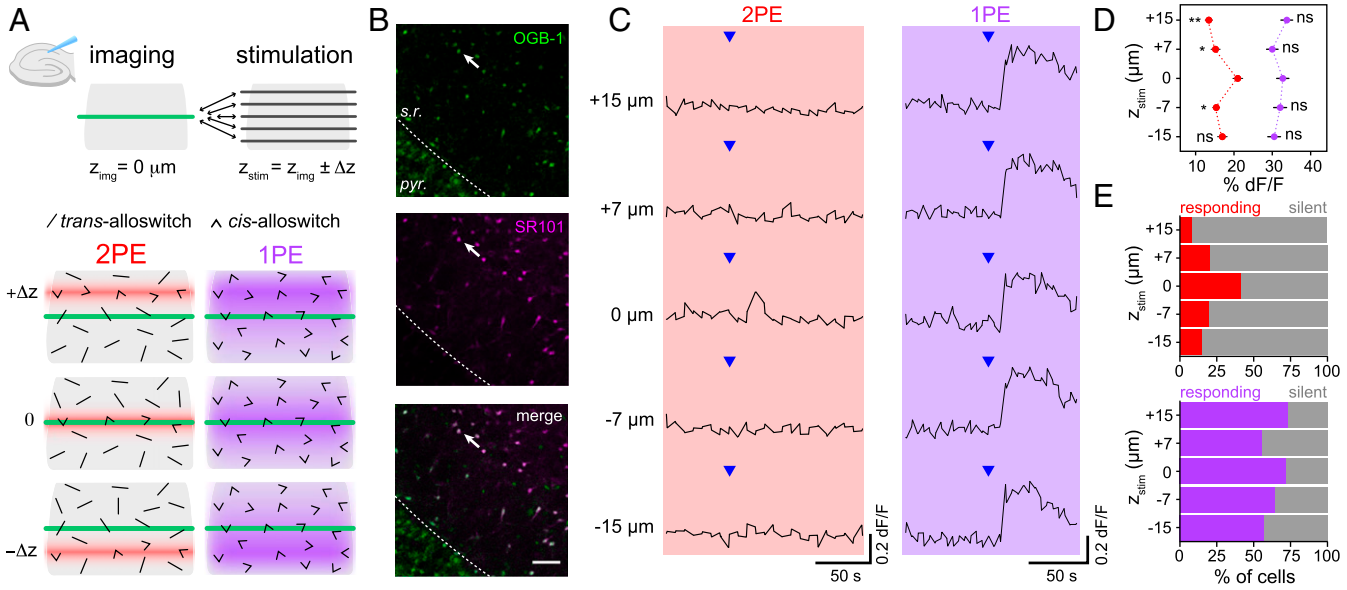

Fig. 7. Two-photon excitation of bath-applied alloswitch enables axially resolved activation of endogenous $mGlu_5$ in brain slices. (*A*) Experimental design for imaging cells in the CA1 region of a rat acute brain slice at one plane (imaging plane, Z_{img} = 0 μm) while 2PE (780 nm) or 1PE (405 nm) of alloswitch (10 μM) is performed at different positions along the *z* axis ($Z_{stim} = Z_{img} \pm \Delta Z$, with ΔZ = 0, 7, 15 μm) by moving the microscope objective between consecutive image acquisitions. Photostimulation started from the farthest Z_{stim} (+15 or −15 μm) and sequentially approached Z_{img} in both directions. Pipette position for agonist ejection is fixed. Photoswitching to *cis*-alloswitch at 2PE is restricted to a limited tissue volume compared with 1PE, and only photoactivates imaged cells when ΔZ = 0. (*B*) Fluorescent images of the pyramidal cell layer (pyr.) and stratum radiatum (s.r.) of the CA1 of the hippocampus in a slice bulk-loaded with OGB-1 for Ca^{2+} imaging (*Top*) and colabeled with the astrocytic marker SR101 (*Middle*) included in the pipette solution. The merged image (*Bottom*) allows classification of cells as astrocytes or neurons (see quantification of cell types in *SI Appendix*, Fig. S6). Arrows indicate cells displayed in *C*. (Scale bar, 50 μm.) (*C*) Representative Ca^{2+} responses from one cell of the stratum radiatum (arrows in *B*). Agonist (blue arrowheads, 1 mM DHPG) was locally ejected and changes in OGB-1 fluorescence (% dF/F) at Z_{img} were monitored during 2PE (red box) and 1PE of alloswitch (violet box) at all indicated axial distances. See imaging/photostimulation schematics and control ejections with/without alloswitch and before/after photostimulations (*SI Appendix*, Fig. S7). (*D*) Average peak amplitudes of Ca^{2+} responses at Z_{img} while photostimulating cells at the indicated axial distances. Peak amplitudes of responses acquired at Z_{img} while photostimulating at $Z_{stim} = \pm 7, \pm 15$ were compared with that of Z_{stim} = 0. Two-photon excitation of alloswitch evoked the largest response when Z_{stim} = 0 (in %dF/F, 13.5 ± 1.0, 15.2 ± 1.2, 21.0 ± 1.3, 15.4 ± 0.9, and 17. 0 ± 1.3, respectively). Single-photon excitation responses did not significantly change with Z_{stim} (in %dF/F, 33.8 ± 1.6, 30.0 ± 1.5, 32.7 ± 1.6, 32.0 ± 1.7, and 30.5 ± 1.7). Data are mean ± SEM; 2-way ANOVA, $*P < 0.05$, $**P < 0.01$; ns, not significant. The resolution for 2PE of alloswitch achieved under these experimental conditions was obtained by fitting to a Gaussian function (FWHM; 6.2 ± 2.2 μm). (*E*) Percentages of silent (gray) or responding cells (colored) at Z_{img} during 2PE and 1PE of alloswitch at each indicated Z_{stim}. The number of responding cells within the imaged area (0.1 mm^2) during 2PE was 9, 23, 47, 22, and 17 (*Upper*; 8%, 20%, 41%, 19%, and 15%) and during 1PE, 83, 63, 82, 73, and 65 (*Lower*; 73%, 55%, 72%, 64%, and 57%). For percentage of cells responding to 2PE, the FWHM of the Gaussian fitting was 10.3 ± 2.3 μm.

onto the apical dendritic arbor, but not the somatic region, of CA1 neurons can induce persistent sodium conductance (43). However, further spatially resolved insight was not possible, because puffing of the agonist evokes an extended recruitment of receptors while it travels away from the ejection site.

Because the experiments of Figs. 1–7 validate the use of alloswitch combined with 2PE for the localized activation of $mGlu_5$ receptors in 3D tissues, we aimed to employ the unique potential of this technique to investigate the intracellular signaling downstream of $mGlu_5$ receptors in apical and basal dendrites of CA1 neurons. To do this, we bathed cultured rat hippocampal slices expressing DsRed2 and GCaMP6s (as morphology and calcium reporters, respectively) with alloswitch and DHPG to silence $mGlu_5$ receptors (Fig. 8 *A* and *B*) (LY367385 was included in the bath to prevent $mGlu_1$ activation by DHPG). Silencing of $mGlu_5$ was then removed locally by sequentially targeting 2PE to the basal or apical dendritic compartment of the same pyramidal neuron (Fig. 8 *B*, *Right*). Rescue of $mGlu_5$ receptors in the apical, but not basal, dendritic segment stemming from the neuron resulted in a broad Ca^{2+} rise, affecting mainly the apical region ($P = 0.032$), but to a lesser extent also the soma and basal compartments (Fig. 8 *C* and *D*). The photoresponse latency in organotypic slice experiments performed in the presence of DHPG was measured after the 2PE illumination onset and yielded 23 ± 8 s (4 cells), similar to the latency obtained in acute slices.

Discussion

Existing strategies to elucidate protein function include genetic or pharmacological manipulations; however, both show several limitations. In the first place, genetic targeting is usually aimed at either ablation of protein expression via antisense oligonucleotides, or disrupting the gene encoding for the protein under study, either in the whole organism in knockouts or at specific ages, tissues, and cell types in conditional knockouts. All experimental observations based on these approaches rely on the indirect effects derived from receptor absence, which are wider and less specific than the direct effects of receptor activation/inhibition. Recent advances in these fields have raised concerns about the mechanisms enabled by genetically modified organisms to compensate for or adapt to protein loss (44), and how such compensatory mechanisms influence the outcomes of experimental observations is largely underestimated (45). Second, pharmacological blockade of protein function is a fast, simple, and flexible methodology that is routinely used to manipulate receptor activity without altering genes or protein levels. Although continued efforts in drug development are filling the gaps in the availability of potent and receptor-selective ligands, pharmacological agents are still limited by the relatively slow time course of compound application, diffusion, and removal, reducing their experimental versatility (3). Strategies to constrain the spatial and temporal functions of drugs include localized perfusion and fast delivery systems, and conjugation with macromolecules (46). However, these methods fall short of the spatiotemporal scales relevant to neural function, such as the micrometric dimensions of dendritic spines and astrocytic processes, neuronal action potentials, and astrocytic Ca^{2+} signals lasting milliseconds to seconds. In contrast, photopharmacology allows control of drug activity at the spatiotemporal coordinates of the patterned illumination defined by the user. It encompasses a new class of diffusible ligands that are light-regulated and enable turning on and off the activity of endogenous receptors at physiological locations and time-scales.

Advanced imaging methods using patterned illumination by multiphoton microscopy with femtosecond pulsed lasers (23) enabled imaging the cortical activity in mice at millimeter depths (47). Recent progress, including scanless spatial light modulation and holographic patterning (48, 49) as well as temporal focusing techniques (50), are currently being exploited for optogenetic stimulation (51–55). However, applications to photopharmacology have been reported only in a few cases, and focused on molecular aspects rather than functional outcomes (15, 26, 27).

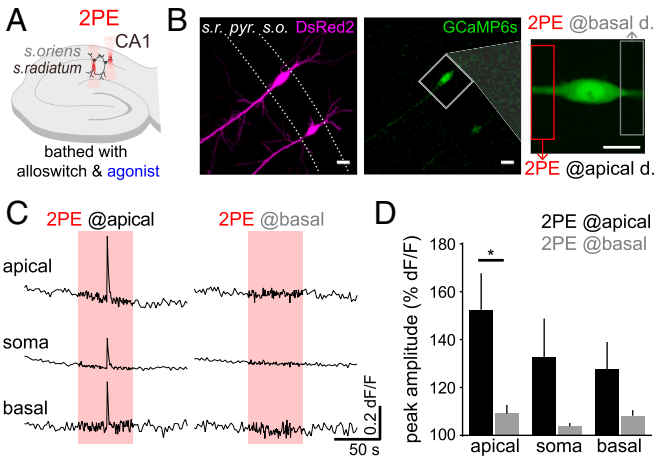

Fig. 8. Two-photon pharmacology with alloswitch allows functional mapping of $mGlu_5$ receptors at the subcellular scale in CA1 pyramidal neurons. (*A*) Experimental scheme in organotypic hippocampal slices: slices are bathed with 10 μM alloswitch and 50 μM DHPG (agonist), as well as 100 μM LY367385 to prevent $mGlu_1$ activation. Silencing of $mGlu_5$ by alloswitch is released locally, by targeting 2PE to the stratum oriens or stratum radiatum of CA1 (basal and apical dendritic regions of pyramidal neurons, respectively). (*B*) CA1 pyramidal neurons expressing the Ca^{2+} sensor GCaMP6s (*Center* and *Right*) and DsRed2 (*Left*), and zoomed view (*Right*) of the neuron imaged in *C*. The extent of 2PE is indicated by boxes (12 × 52 μm). (Scale bars, 20 μm.). (*C*) Calcium traces recorded in the somatic, apical and basal dendritic regions, while 2PE of alloswitch (red boxes, 780 nm, 1.5 Hz, 1 min) is confined to the apical (*Left*) or basal (*Right*) dendritic segments. Activation of $mGlu_5$ receptors in the apical, but not basal, dendritic compartment induce broad Ca^{2+} signals in CA1 pyramidal neurons. (*D*) Quantification of Ca^{2+} responses as normalized peak amplitude, measured at the indicated cellular compartment during 2PE at the apical (black) or basal (gray) dendritic compartment. Paired *t* test, $*P = 0.032$; $n = 4$ cells from 3 animals.

To take advantage of the spatiotemporal control of light-regulated drugs using 2PE (2-photon pharmacology, 2PP) we chose alloswitch, whose nanomolar activity and subtype selectivity make it especially suitable to manipulate endogenous receptors in intact neural tissue. Bath application of alloswitch immediately silenced $mGlu_5$ receptors, and 2PE produced rapid and localized rescue of $mGlu_5$ agonist responses. Illumination power, wavelength, and other 2PE conditions can be achieved with commercial pulsed lasers (Fig. 2) and were effective in all tested alloswitch analogs (4 selected from a library of 18) (*SI Appendix*, Fig. S3) (28). Two-photon excitation of alloswitch achieved $mGlu_5$ responses comparable to endogenous activity induced by agonist, yet weaker than 1PE in the same conditions (Fig. 3*D*). Nevertheless, screening the 2PE responses of available photopharmacological analogs (28) and designing new compounds with improved 2PE isomerization efficiency (56) should give rise to a new generation of 2PP-optimized ligands able to transduce complex 3D illumination patterns into selective activation of endogenous receptors in neuronal circuits with total reliability. Compared with caged ligands (57), alloswitch and other reversible photoswitchable compounds provide better receptor subtype selectivity and allow controlling the receptor deactivation rate (4). The thermal relaxation lifetime can be adjusted by molecular design (it is 80 s for alloswitch) but other factors can influence the observed reblock kinetics, which is in the range of tens of seconds. These include compound diffusion in solution and in tissue, and partitioning with membranes.

The efficiency of 2PE of alloswitch observed in our functional study using raster scanning (in Fig. 3 *D*, *Right*, the magnitude of alloswitch 2PE responses is ~50% compared with 1PE responses in cultured cells) is higher than that of other azobenzene-based photoswitches stimulated similarly (15, 26, 27). This effect might be due to the favorable push–pull character of alloswitch molecules, but downstream amplification of the signal by G protein-coupled receptor

effector proteins cannot be ruled out (27). The proportion of cells in the field-of-view responding to 2PE compared with 1PE in brain slices (33%) (Fig. 6 *C*, *Upper*) is in line with that observed in cultured cells (36% at 0 μm) (Fig. 4*D*). This suggests that diffusion of alloswitch isomers in the highly packed brain tissue (58) is not a limiting factor to photocontrol $mGlu_5$ receptor responses, and that improving the 2PE molecular properties of alloswitch should have a direct effect on 2PP performance. Overall, the results of Figs. 5 and 6 demonstrate that the activity of neuronal receptors can be controlled by 2PE of allosteric drugs in intact brain slices. Interestingly, using 1PE of alloswitch, Ca^{2+} responses were recovered in a significantly higher fraction of cells in the field-of-view than those responding to DHPG in the absence of alloswitch (Fig. 5*E*). Similar effects are observed in cell lines (Fig. 3*D*) and have been previously reported (16, 28). In brain slices, these results suggest that pharmacological silencing of $mGlu_5$ receptors followed by rapid photo-rescue in a physiological setting uncovers neglected features of receptor balancing in response to prolonged arrested signaling. Dedicated studies are required to investigate the relevance of this phenomenon, and could be facilitated by developing $mGlu_5$-selective, *cis*-active inhibitors and potentiators.

The quantification of $mGlu_5$ responses yielded an axial resolution for 2PE of alloswitch in acute brain slices between 5 and 10 μm (either quantifying the response %dF/F or the number of responding cells in Fig. 7 *D* and *E*, respectively). These values match well the average size of brain cell somata, and are comparable to those obtained using optogenetic tools (12.5 μm axial resolution with C1V1 channelrhodopsin) (59). In our wide-field, low-magnification fluorescence microscopy movies, fluorescence changes are observed mainly at the cell bodies (Movies S3 and S4). Although the presence of TTX in the bath guaranteed that the Ca^{2+} activity was initiated by resident $mGlu_5$ receptors and not propagated, the resolution obtained with 2PE is still influenced by the spatial distribution of the cells expressing $mGlu_5$ in brain slices, and by the limited sensitivity of chemical dyes to measure Ca^{2+} responses in cellular processes away from the soma. Using GCaMP6s in organotypic brain slices, the effective resolution that can be achieved in 2PP experiments depends on the local density of target receptors, on the 2PE efficacy of the photoswitch and its diffusion and relaxation in tissue, in addition to the optical resolution of the microscope. We have demonstrated subcellular functional responses by 2PE of a region of 12 × 52 μm in the sample plane. Imaging and photostimulation at higher magnifications than those used in the present study leave room to improve the spatial resolution of 2PP. For example, Ca^{2+} in distal dendritic branches or peripheral astrocytic processes could be efficiently monitored using other genetically engineered Ca^{2+} indicators, and $mGlu_5$ targeted using alloswitch molecules by first silencing receptors widely, and then selectively rescuing them by 2PE in micrometric volumes corresponding to single spines or individual astrocyte processes. We further envisage that measurements limited only by the point-spread function of illumination can be achieved using receptor-bound sensors like FRET probes rather than downstream signaling reporters like Ca^{2+} probes. This would enable pharmacologically selective photocontrol of individual spines: for example, elucidating if functional responses can be elicited by activation of postsynaptically expressed $mGlu_5$ receptors.

Alloswitch photoresponses observed in astrocytes and neurons (Fig. 7*B* and *SI Appendix*, Fig. S6) are in agreement with the reported expression of functional $mGlu_5$ in both cell types (39). The slightly lower fraction of neurons (compared with astrocytes) that respond to 2PE compared with 1PE may be due their size and spread of astrocytic branches being larger than the volume effectively illuminated by 2PE, and is in accordance with the high complexity of Ca^{2+} signals displayed by astrocytic compartments (60). Further insights into $mGlu_5$ signaling in neurons and astrocytes could be drawn from higher magnification studies of brain activity with 2PP. For example, our raster-scanned, plane-selective activation of glial and neuronal $mGlu_5$ receptors in intact neural tissue could be enhanced using 2PE holography to achieve full 3D patterned control at the single cell or subcellular scales, and provide an unprecedented view over the spatial spread and time course of endogenous receptor signaling (61, 62).

The robustness of $mGlu_5$ silencing and 2PE-rescue of responses by alloswitch is outstanding both in cultured cells and in brain slices (Figs. 4 and 6). Given the nanomolar potency of *trans*-alloswitch, its ability to completely silence $mGlu_5$ activity was not a matter of concern in any scenario. However, that particular property, together with the expected partial efficacy of 2PE to convert *trans*-alloswitch to the *cis* form, suggested that a large fraction of *trans*-alloswitch would remain in the focal volume, and that it would be surrounded by an even larger pool of *trans*-isomers ready to flood that volume by diffusion. In this context, the fact that $mGlu_5$-specific intracellular signaling can be elicited in the presence of alloswitch during periods of 2PE demonstrates that *trans*- and *cis*-alloswitch do not interfere with one another in these experiments. This could be due in part to limitations in the diffusion of *trans*-alloswitch into the 2PE volume. However, this explanation is unlikely because 2PE of the alloswitch was also observed in cultured cells, where diffusion of molecules is not hindered by anatomical constraints as in neural tissue (58). Another possibility is that $mGlu_5$ receptor-bound *trans*-molecules could be photoconverted to *cis* inside the allosteric binding pocket of the protein, and if photoconversion (picoseconds) was faster than the kinetics of unbinding from the receptor (milliseconds or more) (63, 64), then the 1-nm-wide entrance of the allosteric ligand binding site of $mGlu_5$ (65) might hinder the exit of *cis*-molecules and prevent *trans*-molecules from entering and inhibiting the receptor. This hypothesis could be tested using FRET measurements of receptor conformational changes (66) combined with methods for rapid photoswitching (4).

The latency of 2PE responses is around 30 s in brain slices and 10 s more in cell lines, and the observed differences may be due to a different local density of receptors in cell lines compared with slices, to the different method used for delivery of agonist (bathed versus ejected), or to a different effective concentration of alloswitch as a result of limited diffusion or partitioning in brain tissue. In our experiments the intensity of illumination was relatively low to prioritize cell health, but higher powers should substantially reduce the latency of responses in both scenarios.

Caged compounds are another class of photopharmacological agents that can be activated using 2PE. Because irreversibly photoreleased molecules cannot be deactivated, their effect can only cease by diffusion in the surrounding medium (which is maximal when the 2PE volume is small) or by neurotransmitter removal via enzymatic hydrolysis or reuptake inside cells. In contrast, reversible photoswitches like alloswitch are in steady-state equilibrium between their active and inactive isomers. This equilibrium can be displaced in either direction by means of illumination or thermal relaxation. As the diffusion of molecules is constrained at the nanoscale in the synaptic cleft (58), reversibility constitutes an important advantage of photoswitching compared with irreversible uncaging of ligands.

Two-photon pharmacology with alloswitch has the potential to be translated to in vivo studies, based on our previous work indicating that alloswitch is readily available in the nervous tissue of behaving animals (16). The requirement of alloswitch along with the orthosteric agonist in cell culture and slices could be challenging in vivo due to the limited solubility and bioavailability of selective agonists for the $mGlu_5$ receptor subtype. However, the use of an allosteric ligand like alloswitch in our demonstration of 2PP is intended to conveniently modulate the effect of the endogenous orthosteric ligand (glutamate), which is naturally available at synaptic or perisynaptic sites where $mGlu_5$ receptors are localized. As shown in our previous work in tadpoles (16), such orthogonal regulation does not require administration of orthosteric ligands and underlines the physiological relevance of 2PP.

Signaling pathways involving $mGlu_5$ function govern important physiological processes whose mechanisms remain controversial due to the lack of suitable experimental tools to study them. Here, we applied 2PP of alloswitch to investigate functionally the subcellular localization of $mGlu_5$ receptors in CA1 pyramidal cells (Fig. 8), and—thanks to its compatibility with sensitive Ca^{2+}

indicators—we were able to map the extent of signaling downstream of $mGlu_5$ activation, when this is confined to the apical dendritic compartment. The pharmacologically selective and spatiotemporally controlled activation of $mGlu_5$ in intact brain tissue that is demonstrated here is a first step to use 2PP with alloswitch to address several biological questions. For example, in the developing cortex, is glutamatergic signaling inducing specific spatiotemporal patterns of $mGlu_5$ activation that organize neurons and glia into functional networks (67, 68)? After development, what patterns of $mGlu_5$ activation drive synaptic plasticity (69), homeostatic scaling (70), and regulation of basal transmission (71)? In addition, what are the roles played by the different $mGlu_5$-expressing cell types of the hippocampus in the mechanism of mGluR-dependent long-term depression (72)? How many spines, dendritic branches, or cells are involved in synaptic plasticity (73)? Further increasing the resolution of photostimulation will allow studying how $mGlu_5$ receptors expressed on organelles (including nuclear membranes and other subcellular localizations) (74) contribute to the complexity of canonical and noncanonical signaling pathways activated downstream of $mGlu_5$ (75). Thus, 2PP in physiologically relevant settings, such as brain slices, or in anesthetized and awake animals will be an invaluable tool to understand how neurotransmitter receptors of neurons and glia function in the intact brain.

Conclusions

We have demonstrated that photoswitchable allosteric modulators of mGlu5 receptor activity (alloswitch and its analogs) can be effectively photoisomerized using pulsed near-infrared lasers (2PE) in cultured cells and acute brain slices. Combining potent and subtype-selective photopharmacology with 2PE allows us to silence and photo-rescue endogenous receptors rapidly and reversibly. We calculated the axial plane selectivity of 2PE of a photoswitchable ligand in brain slices (10 μm), and this value corresponds to the size of single neuronal and astrocytic somata. Thus, photoswitchable ligands of endogenous receptors allow high-resolution 2PP, despite diffusion in neural tissue. This method does not require any genetic manipulation, and is readily applicable to intact tissue. The efficiency of alloswitch to induce $mGlu_5$ photoresponses using 2PE is higher than that of other azobenzene-based photoswitches. All alloswitch analogs tested in this study were found to be 2PE-active, which should allow further optimization of their 2PE properties. In addition, the activation of neuronal and glial $mGlu_5$ receptors can be traced separately in intact tissue, which opens the way to study their distinct physiological roles with unprecedented spatiotemporal resolution and tissue depth. In this way, 2PP is a useful and versatile addition to the molecular toolbox to study neural function.

Materials and Methods

Diffusible Photoswitches, Cell Culture, and Brain Slices.

Compounds. Alloswitch (16) and compounds **1c-d**, **1j**, and **6** (28) were obtained as previously described. Other drugs were purchased from Tocris.

Cell culture. HEK cells transiently expressing $mGlu_5$-eYFP, or $mGlu_5$ and GCaMP6s (1:1), were imaged 48–96 h after transfection. Cells expressing $mGlu_5$-eYFP were loaded with Fura-2 AM before experiments. Bath solution contained: 140 mM NaCl, 5.4 mM KCl, 1 mM $MgCl_2$, 10 mM Hepes, 10 mM D-glucose, and 2 mM $CaCl_2$ (pH 7.40).

Acute brain slices. All animal procedures were approved by the Animal Experimentation Ethics Committee at the University of Barcelona (OB-432/16). Acute coronal slices (350-μm thick) containing the hippocampus were obtained from 6 to 15 postnatal days (P6–15) Sprague-Dawley rats (Envigo) using a vibrating-knife microtome (1000S Vibratome, Leica) in oxygenated, ice-cold, high-sucrose cutting solution. Acute slices were recovered (1 h, room temperature) in oxygenated artificial cerebrospinal fluid (aCSF) containing 126 mM NaCl, 26 mM $NaHCO_3$, 1.145 mM NaH_2PO_4, 3 mM KCl, 10 mM glucose, 2 mM $MgSO_4$, and 2 mM $CaCl_2$, before OGB-1 AM loading with Pluronic F-127.

Organotypic hippocampal slices. Slices (400-μm thick) were obtained from P7 Sprague-Dawley rats (Janvier Labs) using a tissue chopper and cultured for 5–7 d in vitro until biolistically transfected with GCaMP6s and DsRed2 (Addgene). Slices were used for experiments at days in vitro 7–14 in oxygenated aCSF containing: 119 mM NaCl, 2.5 mM KCl, 2 mM $CaCl_2$, 1 mM $MgCl_2$, 26 mM $NaHCO_3$, 1 mM NaH_2PO_4, and 11 mM glucose.

Photostimulation and Imaging.

Imaging setup. All experiments were performed using an inverted, laser-scanning confocal microscope (TCS SP5, Leica Microsystems) equipped with an infrared pulsed laser (MaiTai Wide Band, 710–990 nm; Spectra Physics) and continuous-wave lasers (405-nm laser diode and Argon laser; LASOS).

Drugs for slice experiments. In acute brain slices, $mGlu_5$ receptors were stimulated by brief (1 s) pressure-ejection of the orthosteric agonist DHPG (1 mM). The astrocytic marker SR101 was included in the pipette solution. aCSF was supplemented with LY367385 (100 μM) to prevent $mGlu_1$ activation by DHPG, TTX (1 μM) to prevent Ca^{2+} signals due to neuronal firing before experiments, and alloswitch (10 μM), as indicated in figures. For organotypic slices, aCSF was supplemented with alloswitch (10 μM) and LY367385 (100 μM) 10 min before experiments, and DHPG (50 μM) was supplemented directly in the bathed aCSF.

Imaging. Fura-2 was imaged at 0.2 Hz in the single-wavelength, non-ratiometric modality (*SI Appendix*, Fig. S1), setting the pulsed laser (760–820 nm) at low power (3 mW) to minimize potential *trans*-to-*cis* isomerization of alloswitch due to imaging. GCaMP6s and OGB-1 were imaged at 488 nm at low power to avoid unwanted *cis*-to-*trans* photoisomerization of alloswitch (in cells: 100 nW, 0.2 Hz in cells; in acute slices: <5.2 μW, 1–0.33 Hz; in organotypic slices: <3 μW, 0.5 Hz).

Photostimulation. Photostimulation at 1PE or 2PE was achieved using the lasers indicated above (1PE: 405 nm, 2 μW in cultured cells, 58–98 μW in acute slices; 2PE: 760–820 nm, 12 mW in Fura-2–loaded cells, 20 mW for GCaMP6s-expressing cells, 25 mW for slices) by single or multiple (<13) raster-scans of the field-of-view interleaved between 2 consecutive image acquisitions of either Fura-2, GCaMP6s, or OGB-1. For local 2PE in organotypic slices, the basal or apical dendritic segment was photostimulated (780 nm, 12 mW) on a 12 × 52-μm area.

Data analysis and statistics. Calcium traces were extracted using ImageJ and represented as dF/F. For acute slices, analysis was assisted with a macro written at ADMCF (Advanced Digital Microscopy Core Facility, IRBB; code available online at https://sites.google.com/a/irbbarcelona.org/adm/image-j-fiji#TOC-Somata-segmentation-and-time-response-analysis-in-acute-rodent-brain-slices-). Data are represented as mean ± SEM and available upon request; statistics are indicated in figure captions.

See *SI Appendix* for details on culture and slice protocols, image acquisition, photostimulation, data analysis, and inclusion criteria.

ACKNOWLEDGMENTS. We thank Jordi Hernando (Autonomous University of Barcelona) for useful discussions on 2-photon excitation; Pere Català (Utrecht University) for help with GCaMP; Francisco Ciruela (University of Barcelona) for $mGlu_5$-eYFP plasmid; Erin Schuman and Stephan Junek (Max Planck Institute for Brain Research, Frankfurt) for preliminary 2-photon excitation experiments; and Ashraf Muhaisen (University of Barcelona) for help with slicing. This research received funding from European Union Research and Innovation Programme Horizon 2020 [Human Brain Project SGA2 Grant Agreement 785907 (WaveScalES)], European Research ERA-Net SynBio programme (Modulightor project), and financial support from Agency for Management of University and Research Grants/Generalitat de Catalunya (CERCA Programme; 2017-SGR-1442 project), Fonds Européen de Développement Économique et Régional (FEDER) funds, Ministry of Economy and Competitiveness (MINECO)/FEDER (Grant CTQ2016-80066-R), and the Fundaluce foundation. S.P. was supported by an FI fellowship from the Agency for Management of University and Research Grants/Generalitat de Catalunya (2014FI_B2 00160). H.L. was supported by an Institute for Bioengineering of Catalonia Severo Ochoa International PhD Programme fellowship from MINECO. M.B. was supported by a H2020-MSCA-IF Reintegration Grant. K.E.P. receives support from NIH/National Institute of Neurological Disorders and Stroke Grant R01NS099254 and NSF Biophotonics Grant 1604544. E.S. receives support from MINECO (Grant SAF2016-7426).

1. H. Kim, J. S. Kim, A guide to genome engineering with programmable nucleases. *Nat. Rev. Genet.* **15**, 321–334 (2014).
2. M. Ghildiyal, P. D. Zamore, Small silencing RNAs: An expanding universe. *Nat. Rev. Genet.* **10**, 94–108 (2009).
3. M. Behar, D. Barken, S. L. Werner, A. Hoffmann, The dynamics of signaling as a pharmacological target. *Cell* **155**, 448–461 (2013).
4. A. Reiner, E. Y. Isacoff, Tethered ligands reveal glutamate receptor desensitization depends on subunit occupancy. *Nat. Chem. Biol.* **10**, 273–280 (2014).
5. W. A. Velema, W. Szymanski, B. L. Feringa, Photopharmacology: Beyond proof of principle. *J. Am. Chem. Soc.* **136**, 2178–2191 (2014).
6. M. A. Kienzler, E. Y. Isacoff, Precise modulation of neuronal activity with synthetic photoswitchable ligands. *Curr. Opin. Neurobiol.* **45**, 202–209 (2017).

7. K. A. Schaefer *et al*., Unexpected mutations after CRISPR-Cas9 editing in vivo. *Nat. Methods* **14**, 547–548 (2017).
8. G. Miesenböck, Optogenetic control of cells and circuits. *Annu. Rev. Cell Dev. Biol.* **27**, 731–758 (2011).
9. B. R. Rost, F. Schneider-Warme, D. Schmitz, P. Hegemann, Optogenetic tools for subcellular applications in neuroscience. *Neuron* **96**, 572–603 (2017).
10. T. Miyashita, Y. R. Shao, J. Chung, O. Pourzia, D. E. Feldman, Long-term channelrhodopsin-2 (ChR2) expression can induce abnormal axonal morphology and targeting in cerebral cortex. *Front. Neural Circuits* **7**, 8 (2013).
11. W. Wu *et al*., Increased threshold of short-latency motor evoked potentials in transgenic mice expressing Channelrhodopsin-2. *PLoS One* **12**, e0178803 (2017).
12. M. Volgraf *et al*., Reversibly caged glutamate: A photochromic agonist of ionotropic glutamate receptors. *J. Am. Chem. Soc.* **129**, 260–261 (2007).
13. P. Stawski, M. Sumser, D. Trauner, A photochromic agonist of AMPA receptors. *Angew. Chem. Int. Ed. Engl.* **51**, 5748–5751 (2012).
14. D. M. Barber *et al*., Optical control of AMPA receptors using a photoswitchable quinoxaline-2,3-dione antagonist. *Chem. Sci. (Camb.)* **8**, 611–615 (2017).
15. L. Laprell *et al*., Optical control of NMDA receptors with a diffusible photoswitch. *Nat. Commun.* **6**, 8076 (2015).
16. S. Pittolo *et al*., An allosteric modulator to control endogenous G protein-coupled receptors with light. *Nat. Chem. Biol.* **10**, 813–815 (2014).
17. X. Rovira *et al*., OptoGluNAM4.1, a photoswitchable allosteric antagonist for real-time control of mGlu4 receptor activity. *Cell Chem. Biol.* **23**, 929–934 (2016).
18. M. R. Banghart, B. L. Sabatini, Photoactivatable neuropeptides for spatiotemporally precise delivery of opioids in neural tissue. *Neuron* **73**, 249–259 (2012).
19. M. Schönberger, D. Trauner, A photochromic agonist for μ-opioid receptors. *Angew. Chem. Int. Ed. Engl.* **53**, 3264–3267 (2014).
20. M. Stein *et al*., Azo-propofols: Photochromic potentiators of GABA(A) receptors. *Angew. Chem. Int. Ed. Engl.* **51**, 10500–10504 (2012).
21. A. Damijonaitis *et al*., AzoCholine enables optical control of alpha 7 nicotinic acetylcholine receptors in neural networks. *ACS Chem. Neurosci.* **6**, 701–707 (2015).
22. M. I. Bahamonde *et al*., Photomodulation of G protein-coupled adenosine receptors by a novel light-switchable ligand. *Bioconjug. Chem.* **25**, 1847–1854 (2014).
23. W. Denk, J. H. Strickler, W. W. Webb, Two-photon laser scanning fluorescence microscopy. *Science* **248**, 73–76 (1990).
24. K. Svoboda, R. Yasuda, Principles of two-photon excitation microscopy and its applications to neuroscience. *Neuron* **50**, 823–839 (2006).
25. A. M. Packer, B. Roska, M. Häusser, Targeting neurons and photons for optogenetics. *Nat. Neurosci.* **16**, 805–815 (2013).
26. M. Izquierdo-Serra *et al*., Two-photon neuronal and astrocytic stimulation with azobenzene-based photoswitches. *J. Am. Chem. Soc.* **136**, 8693–8701 (2014).
27. E. C. Carroll *et al*., Two-photon brightness of azobenzene photoswitches designed for glutamate receptor optogenetics. *Proc. Natl. Acad. Sci. U.S.A.* **112**, E776–E785 (2015).
28. X. Gómez-Santacana *et al*., Illuminating phenylazopyridines to photoswitch metabotropic glutamate receptors: From the flask to the animals. *ACS Cent. Sci.* **3**, 81–91 (2017).
29. K. M. Huber, M. S. Kayser, M. F. Bear, Role for rapid dendritic protein synthesis in hippocampal mGluR-dependent long-term depression. *Science* **288**, 1254–1257 (2000).
30. X. Wang *et al*., Altered mGluR5-Homer scaffolds and corticostriatal connectivity in a Shank3 complete knockout model of autism. *Nat. Commun.* **7**, 11459 (2016).
31. E. Aloisi *et al*., Altered surface mGluR5 dynamics provoke synaptic NMDAR dysfunction and cognitive defects in Fmr1 knockout mice. *Nat. Commun.* **8**, 1103 (2017).
32. N. Matosin, F. Fernandez-Enright, J. S. Lum, K. A. Newell, Shifting towards a model of mGluR5 dysregulation in schizophrenia: Consequences for future schizophrenia treatment. *Neuropharmacology* **115**, 73–91 (2017).
33. S. Shin *et al*., mGluR5 in the nucleus accumbens is critical for promoting resilience to chronic stress. *Nat. Neurosci.* **18**, 1017–1024 (2015).
34. L. T. Haas *et al*., Silent allosteric modulation of mGluR5 maintains glutamate signaling while rescuing Alzheimer's mouse phenotypes. *Cell Rep.* **20**, 76–88 (2017).
35. D. G. Ferreira *et al*., α-Synuclein interacts with PrP^C to induce cognitive impairment through mGluR5 and NMDAR2B. *Nat. Neurosci.* **20**, 1569–1579 (2017).
36. C. Xu, W. R. Zipfel, Multiphoton excitation of fluorescent probes. *Cold Spring Harb. Protoc.* **2015**, 250–258 (2015).
37. T. W. Chen *et al*., Ultrasensitive fluorescent proteins for imaging neuronal activity. *Nature* **499**, 295–300 (2013).
38. M. S. Nash *et al*., Determinants of metabotropic glutamate receptor-5-mediated Ca2+ and inositol 1,4,5-trisphosphate oscillation frequency. Receptor density versus agonist concentration. *J. Biol. Chem.* **277**, 35947–35960 (2002).
39. W. Sun *et al*., Glutamate-dependent neuroglial calcium signaling differs between young and adult brain. *Science* **339**, 197–200 (2013).
40. C. Romano *et al*., Distribution of metabotropic glutamate receptor mGluR5 immunoreactivity in rat brain. *J. Comp. Neurol.* **355**, 455–469 (1995).
41. R. Basu, *et al*., Heterophilic type II cadherins are required for high-magnitude synaptic potentiation in the hippocampus. *Neuron* **96**, 160–176.e8 (2017). Erratum in: *Neuron* **98**, 658–668 (2018).
42. W. Fan, Group I metabotropic glutamate receptors modulate late phase long-term potentiation in hippocampal CA1 pyramidal neurons: Comparison of apical and basal dendrites. *Neurosci. Lett.* **553**, 132–137 (2013).
43. W. Yu *et al*., mGluR5-dependent modulation of dendritic excitability in CA1 pyramidal neurons mediated by enhancement of persistent Na^+ currents. *J. Physiol.* **596**, 4141–4156 (2018).
44. A. Rossi *et al*., Genetic compensation induced by deleterious mutations but not gene knockdowns. *Nature* **524**, 230–233 (2015).
45. M. A. El-Brolosy, D. Y. R. Stainier, Genetic compensation: A phenomenon in search of mechanisms. *PLoS Genet.* **13**, e1006780 (2017).
46. A. Kakkar, G. Traverso, O. C. Farokhzad, R. Weissleder, R. Langer, Evolution of macromolecular complexity in drug delivery systems. *Nat. Rev. Chem.* **1**, 0063 (2017).
47. W. Mittmann *et al*., Two-photon calcium imaging of evoked activity from L5 somatosensory neurons in vivo. *Nat. Neurosci.* **14**, 1089–1093 (2011).
48. V. Nikolenko *et al*., SLM microscopy: Scanless two-photon imaging and photostimulation with spatial light modulators. *Front. Neural Circuits* **2**, 5 (2008).
49. F. Anselmi, C. Ventalon, A. Bègue, D. Ogden, V. Emiliani, Three-dimensional imaging and photostimulation by remote-focusing and holographic light patterning. *Proc. Natl. Acad. Sci. U.S.A.* **108**, 19504–19509 (2011).
50. E. Papagiakoumou *et al*., Scanless two-photon excitation of channelrhodopsin-2. *Nat. Methods* **7**, 848–854 (2010).
51. M. Dal Maschio, J. C. Donovan, T. O. Helmbrecht, H. Baier, Linking neurons to network function and behavior by two-photon holographic optogenetics and volumetric imaging. *Neuron* **94**, 774–789.e5 (2017).
52. R. Prevedel *et al*., Fast volumetric calcium imaging across multiple cortical layers using sculpted light. *Nat. Methods* **13**, 1021–1028 (2016).
53. A. Forli *et al*., Two-photon bidirectional control and imaging of neuronal excitability with high spatial resolution in vivo. *Cell Rep.* **22**, 3087–3098 (2018).
54. O. A. Shemesh *et al*., Temporally precise single-cell-resolution optogenetics. *Nat. Neurosci.* **20**, 1796–1806 (2017).
55. A. R. Mardinly *et al*., Precise multimodal optical control of neural ensemble activity. *Nat. Neurosci.* **21**, 881–893 (2018).
56. G. Cabré *et al*., Rationally designed azobenzene photoswitches for efficient two-photon neuronal excitation. *Nat. Commun.* **10**, 907 (2019).
57. G. C. Ellis-Davies, Two-photon microscopy for chemical neuroscience. *ACS Chem. Neurosci.* **2**, 185–197 (2011).
58. K. Zheng *et al*., Nanoscale diffusion in the synaptic cleft and beyond measured with time-resolved fluorescence anisotropy imaging. *Sci. Rep.* **7**, 42022 (2017).
59. R. Prakash *et al*., Two-photon optogenetic toolbox for fast inhibition, excitation and bistable modulation. *Nat. Methods* **9**, 1171–1179 (2012).
60. A. Volterra, N. Liaudet, I. Savtchouk, Astrocyte Ca^{2+} signalling: An unexpected complexity. *Nat. Rev. Neurosci.* **15**, 327–335 (2014).
61. M. J. Lohse, S. Nuber, C. Hoffmann, Fluorescence/bioluminescence resonance energy transfer techniques to study G-protein-coupled receptor activation and signaling. *Pharmacol. Rev.* **64**, 299–336 (2012).
62. B. N. Kholodenko, J. F. Hancock, W. Kolch, Signalling ballet in space and time. *Nat. Rev. Mol. Cell Biol.* **11**, 414–426 (2010).
63. P. Tiwary, V. Limongelli, M. Salvalaglio, M. Parrinello, Kinetics of protein-ligand unbinding: Predicting pathways, rates, and rate-limiting steps. *Proc. Natl. Acad. Sci. U.S.A.* **112**, E386–E391 (2015).
64. S. Núñez, J. Venhorst, C. G. Kruse, Target-drug interactions: First principles and their application to drug discovery. *Drug Discov. Today* **17**, 10–22 (2012).
65. A. S. Doré *et al*., Structure of class C GPCR metabotropic glutamate receptor 5 transmembrane domain. *Nature* **511**, 557–562 (2014).
66. V. Hlavackova *et al*., Sequential inter- and intrasubunit rearrangements during activation of dimeric metabotropic glutamate receptor 1. *Sci. Signal.* **5**, ra59 (2012).
67. L. S. Wijetunge, S. M. Till, T. H. Gillingwater, C. A. Ingham, P. C. Kind, mGluR5 regulates glutamate-dependent development of the mouse somatosensory cortex. *J. Neurosci.* **28**, 13028–13037 (2008).
68. L. Morel, H. Higashimori, M. Tolman, Y. Yang, VGluT1+ neuronal glutamatergic signaling regulates postnatal developmental maturation of cortical protoplasmic astroglia. *J. Neurosci.* **34**, 10950–10962 (2014).
69. C. Lüscher, K. M. Huber, Group 1 mGluR-dependent synaptic long-term depression: Mechanisms and implications for circuitry and disease. *Neuron* **65**, 445–459 (2010).
70. G. H. Diering *et al*., Homer1a drives homeostatic scaling-down of excitatory synapses during sleep. *Science* **355**, 511–515 (2017).
71. A. Panatier *et al*., Astrocytes are endogenous regulators of basal transmission at central synapses. *Cell* **146**, 785–798 (2011).
72. H. Hagena, D. Manahan-Vaughan, mGlu5 acts as a switch for opposing forms of synaptic plasticity at mossy fiber-CA3 and commissural associational-CA3 synapses. *J. Neurosci.* **35**, 4999–5006 (2015).
73. W. C. Oh, L. K. Parajuli, K. Zito, Heterosynaptic structural plasticity on local dendritic segments of hippocampal CA1 neurons. *Cell Rep.* **10**, 162–169 (2015).
74. Y. I. Jong, S. K. Harmon, K. L. O'Malley, Intracellular GPCRs play key roles in synaptic plasticity. *ACS Chem. Neurosci.* **9**, 2162–2172 (2018).
75. L. J. Stoppel *et al*., β-Arrestin2 couples metabotropic glutamate receptor 5 to neuronal protein synthesis and is a potential target to treat fragile X. *Cell Rep.* **18**, 2807–2814 (2017).